BIOPHYSICS

Homeocurvature adaptation of phospholipids to pressure in deep-sea invertebrates

Jacob R. Winnikoff[1,2,3,4]*, Daniel Milshteyn[1], Sasiri J. Vargas-Urbano[5], Miguel A. Pedraza-Joya[5], Aaron M. Armando[6], Oswald Quehenberger[6], Alexander Sodt[7], Richard E. Gillilan[8], Edward A. Dennis[1,6], Edward Lyman[5], Steven H. D. Haddock[3,4], Itay Budin[1]*

Hydrostatic pressure increases with depth in the ocean, but little is known about the molecular bases of biological pressure tolerance. We describe a mode of pressure adaptation in comb jellies (ctenophores) that also constrains these animals' depth range. Structural analysis of deep-sea ctenophore lipids shows that they form a nonbilayer phase at pressures under which the phase is not typically stable. Lipidomics and all-atom simulations identified phospholipids with strong negative spontaneous curvature, including plasmalogens, as a hallmark of deep-adapted membranes that causes this phase behavior. Synthesis of plasmalogens enhanced pressure tolerance in *Escherichia coli*, whereas low-curvature lipids had the opposite effect. Imaging of ctenophore tissues indicated that the disintegration of deep-sea animals when decompressed could be driven by a phase transition in their phospholipid membranes.

The deep sea encompasses >90% of Earth's habitable volume and is characterized by low temperature and high pressure, with pressure increasing by about 1 bar per 10 m of depth. In contrast to low-temperature adaptation, few specific mechanisms of pressure tolerance in animals are known (*1*). Pressure inhibits high-volume conformations of all biomolecules but has an especially strong effect on lipids because of the high compressibility of their hydrocarbon chains (*2*). Phospholipid membranes generally exist in a liquid-crystalline state known as the fluid lamellar (L_α) phase. When L_α membranes are subjected to increasing pressure, their fluidity decreases, eventually causing a transition to a gel (L_β) phase, like that induced by cold (*3*). For this reason, it has been largely assumed that the phospholipids of marine ectotherms adapt similarly to low temperature and high pressure, following the principle of homeoviscous adaptation (*2*–*5*). However, phospholipid compressibility is also highly anisotropic, meaning that pressure has a strong effect on overall lipid shape. Certain lipids, such as phosphatidylethanolamine (PE), have a conical steric profile, which is rendered more cylindrical by high pressure. Conical lipids are important for membrane protein function (*6*) and favor the formation of nonlamellar intermediates for fusion and fission, such as the inverse hexagonal (H_{II}) phase (*7*).

We investigated high-pressure adaptation in comb jellies (phylum Ctenophora)—soft-bodied, poikilothermic invertebrates that inhabit diverse ocean environments. In situ observations (Fig. 1B) showed that multiple ctenophore lineages adapted independently to various depths (*8*), which makes ctenophores a useful comparative system for studying deep-sea adaptation. In addition to their depth distributions, ctenophores show physiological responses consistent with pressure specialization. When exposed to high pressures, shallow-adapted ctenophores exhibit constant, accelerated beating of their comb rows (movie S1), which leads to eventual shearing (fig. S1, A and B). Loss of motor control in ctenophores and other animals (*9*) could implicate failure at synapses (*10*), which are enriched in cone-shaped lipids (*11*). By contrast, when deep-constrained species are brought isothermally to atmospheric pressure, their tissues disintegrate (Fig. 1A and fig. S1C), a phenomenon also documented across several phyla (*12*, *13*). When imaged by spectral confocal microscopy, ectodermal tissue dissected from deep-constrained ctenophores showed a loss of membrane structure and an abrupt increase in the general polarization (GP) of the fluorescent membrane label C-laurdan—a lipid packing sensor—during disintegration (Fig. 1C). We did not observe this phenomenon in a shallow-constrained ctenophore species, whose habitat extends to the surface, that we collected on the same remotely operated vehicle (ROV) dive. We tested whether pressure effects on cell membranes could underlie ctenophores' physiological tolerances and depth ranges.

Deep-sea membrane lipids form nonlamellar phases when not under high pressure

We probed structural signatures of pressure adaptation in deep-sea membranes by high-pressure small-angle x-ray scattering (HPSAXS) (*14*) and high-pressure fluorescence spectroscopy (HPFS). In HPSAXS, phospholipids produce x-ray scattering patterns (Fig. 2B) from which major phase transitions—i.e., changes in the mobility and arrangement of lipids—can be identified. We used reconstituted polar lipid extracts to map the predominance of the lamellar fluid (L_α), lamellar gel (L_β), and nonlamellar inverted hexagonal (H_{II}) phases across pressure-temperature (P-T) space (Fig. 2C). Within lamellar regimes, membrane fluidity was assessed by HPFS measuring C-laurdan GP (Fig. 2D and fig. S1F). We used these approaches to analyze lipid extracts from five species (eight animals total) that provided sufficient biomass and were native to different domains of depth (0 to 4000 m, collected by SCUBA and ROV) and temperature (0° to 20°C, collected at different latitudes) (Fig. 2A). The comparison of *Beroe cucumis* from Arctic surface waters with Platyctenida sp. T. from the seafloor at ~4000 m was particularly informative because of the similar temperatures but drastically different pressures of their environments. Although these analyses did not sample any single membrane in the organism or account for membrane proteins or osmolytes, they allowed us to compare phase behavior trends that are intrinsic to lipids.

All ctenophore lipid extracts formed an L phase in the native P-T domain of the source animal. Within this phase, membrane fluidity was higher in both deep and shallow cold samples compared with temperate samples, consistent with homeoviscous adaptation (Fig. 2D). Pressure-dependent gel phase transitions ($L_\alpha \rightarrow L_\beta$) were observed at moderate pressures (~200 bar) in lipids from shallow temperate animals and at much higher pressures (>1000 bar) in species from deep water. However, Arctic species inhabiting shallow water, which are adapted to cold but not to high pressure, showed a gel phase transition indistinguishable from that of species that dwell in the deep sea. By contrast, there was a consistent relationship between the animals' native P-T and the nonlamellar phase transition ($L_\alpha \rightarrow H_{II}$) of their lipids. In the species from the deepest environment sampled, decreasing pressure ~200 bar from the native P-T—analogous to moving 2000 m shallower in an isothermal seawater column—caused lipids to invert to H_{II}, which coincided with nonmonotonic trends in C-laurdan GP. Similar habitat-specific patterns were observed in samples from a pair of closely related depth-specialist species that adapted independently to surface and deep waters (fig. S1, D to F). Thus, the deep-sea lipids that we analyzed did not show reduced sensitivity to the $L_\alpha \rightarrow L_\beta$ transition compared with those from shallow, cold-water animals but did have a greater propensity to form the H_{II} phase, which is modulated by lipid shape.

[1]Department of Chemistry and Biochemistry, University of California San Diego, La Jolla, CA 92093, USA. [2]Department of Organismic and Evolutionary Biology, Harvard University, Cambridge, MA 02138, USA. [3]Monterey Bay Aquarium Research Institute, Moss Landing, CA 95039, USA. [4]Department of Ecology and Evolutionary Biology, University of California Santa Cruz, Santa Cruz, CA 95064, USA. [5]Department of Physics and Astronomy, University of Delaware, Newark, DE 19716, USA. [6]Department of Pharmacology, University of California San Diego Health Sciences, La Jolla, CA 92093, USA. [7]Unit on Membrane Chemical Physics, National Institute of Child Health and Human Development, Bethesda, MD 20892, USA. [8]Center for High-Energy X-ray Sciences, Cornell High Energy Synchrotron Source (CHESS), Ithaca, NY 14850, USA.
*Corresponding author. Email: ibudin@ucsd.edu (I.B.); jwinnikoff@g.harvard.edu (J.R.W.)

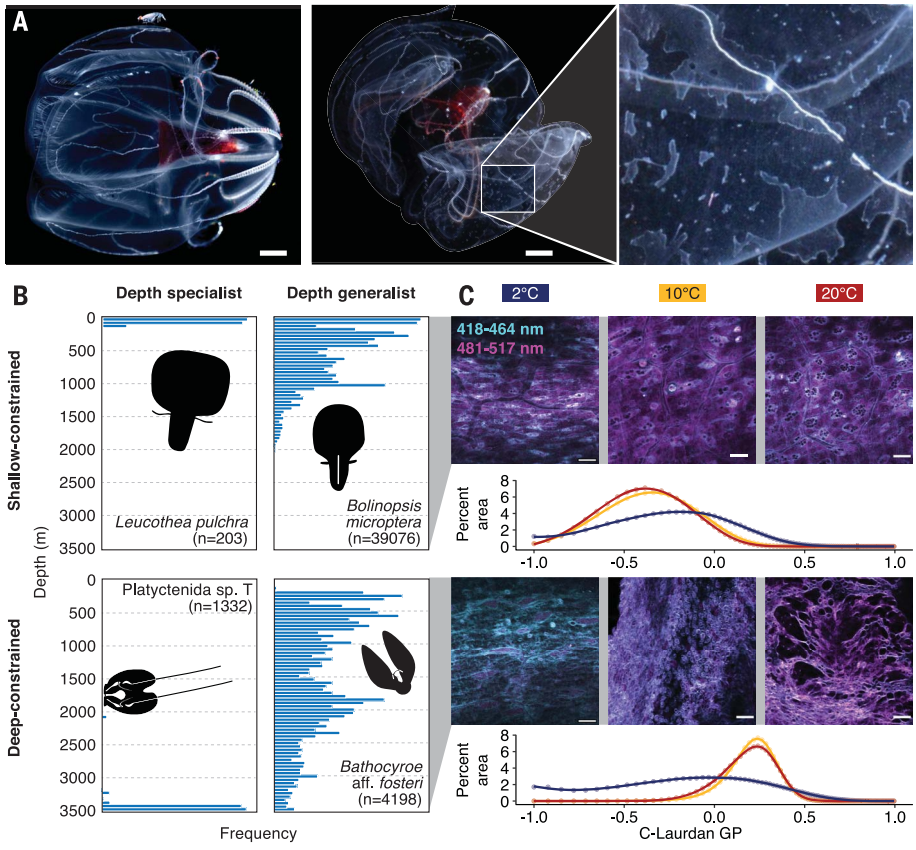

Fig. 1. Ecological and physiological evidence for pressure specialization in ctenophores. (**A**) Disintegration of the deep-constrained ctenophore *Bathocyroe* aff. *fosteri* at atmospheric pressure. The left image was taken in the specimen's native water at 2°C, immediately after recovery from the ROV. The next image is of the same animal and was taken 10 min later at 4°C. Scale bars, 5 mm. Inset (right) shows disintegration of the ectodermal tissue. (**B**) Depth distributions of four ctenophore species with narrow, broad, shallow, and deep depth ranges. (**C**) Live ex vivo tissue mounts stained with solvatochromic C-laurdan membrane label and imaged at increasing temperatures. Images are a composite of two emission ranges, which are used to calculate GP ratios. In *Bolinopsis microptera*, which occurs from 0 to 2000 m, GP value decreases with increasing temperature, indicating a more fluid lamellar phase. In *Bathocyroe*, which occurs down to >3500 m but not shallower than 200 m, GP displays a sharp increase between 2° and 10°C, concurrent with a catastrophic collapse of membrane morphology. This pattern of increase in GP is observed in synthetic lipid systems undergoing inversion (fig. S3C and fig. S8D). Scale bars, 10 μm.

Ctenophore lipids show contrasting adaptations to pressure and cold

To identify the lipids responsible for pressure-specific physical properties, we analyzed ctenophores collected across a 4000-m depth range, as well as from surface waters at tropical, temperate, and Arctic latitudes (Fig. 3A and table S1). This global sampling enabled us to distinguish adaptations to high pressure from those to cold, as temperature also decreases in deeper ocean waters. Phospholipids were the dominant type of polar lipids in all 66 ctenophores sampled (across 17 species), but their headgroup composition displayed divergent relations to high pressure and low temperature (Fig. 3B). Depth was associated with a fivefold increase in the abundance of plasmenyl phosphatidylethanolamine (PPE), which contains an *sn*-1 α-alkenyl ether linkage (*15*). Based on a phylogeny inferred from transcriptomes, depth-associated PPE accumulation appears to have evolved independently at least three times in ctenophores (Fig. 3C). PPE was not associated with cold adaptation independent of depth; in fact, it was more abundant in warm-water, shallow-adapted animals compared with cold-water animals. Animals from shallow, cold water had high amounts of phosphatidylcholine (PC), a cylindrical lipid that increases membrane fluidity and is observed in other cold-adapted poikilotherms (*16*). Outside of phospholipids, ctenophore lipidomes contained small amounts of cholesterol (<5%)—with the notable exception of warm-water animals—and low amounts of sphingomyelin (<0.5%) (fig. S2C).

In addition to headgroups, divergent trends were seen in phospholipid acyl chains. Acyl chain unsaturation followed trends consistent with homeoviscous adaptation: The number of double bonds increased with both increasing depth and decreasing temperature. However, acyl chain length increased in samples from deeper habitats, in contrast to those from cold, shallow water and to the pattern predicted by homeoviscosity (Fig. 3D). P-T trends were most apparent when all acyl chains were averaged; however, the *sn*-1 chains alone exhibited strong signals. The patterns among *sn*-2 chains were similar but not statistically significant (fig. S2A). Acyl chain analysis of lysophosphatidylethanolamine (LPE) also indicated that variation in PPE abundance between samples was not driven by oxidative degradation (fig. S2B). These results indicate that ctenophore lipidomes contain depth-specific adaptations that cannot be fully explained by a need to maintain membrane fluidity. Although our analysis could not resolve ctenophore membrane composition at a subcellular level, the homogeneity of deep and cold-water lipidomes, containing predominantly polyunsaturated PC or PPE, suggests that they do not feature the extensive heterogeneity characteristic of mammalian cell membranes (*17*).

Biophysical measurements and simulations support a homeocurvature adaptation model

We analyzed the pressure-dependent properties of PPE, given that it was the only major depth-correlated lipid class (fig. S2C) and constituted up to 73% of phospholipids in whole bodies—and slightly more in tentacle tissue—from the samples obtained at greatest depth (fig. S2D). The midpoint pressure for the inverted phase transition ($L_\alpha \rightarrow H_{II}$) was higher for liposomes composed of PPE, with either monounsaturated or polyunsaturated *sn*-2 chains, compared with those made of the corresponding PE species. The pressure of the gel phase transition ($L_\alpha \rightarrow L_\beta$) also slightly increased, both shifting and narrowing the fluid lamellar region (Fig. 4A and fig. S3A). Within the lamellar phase, PPE increased membrane fluidity at high pressures (fig. S3B). High membrane fluidity and the ability of lipids to form nonlamellar topologies like H_{II} are thought to be required for membrane fusion (*18*). Accordingly, we found that Ca^{2+}-mediated fusion of liposomes in vitro was inhibited by moderate pressures (100 bar) but that this loss of activity could be restored by substitution of PPE for PE (fig. S4).

In light of the distinctive phase behavior of PPE, we tested whether there is a broader

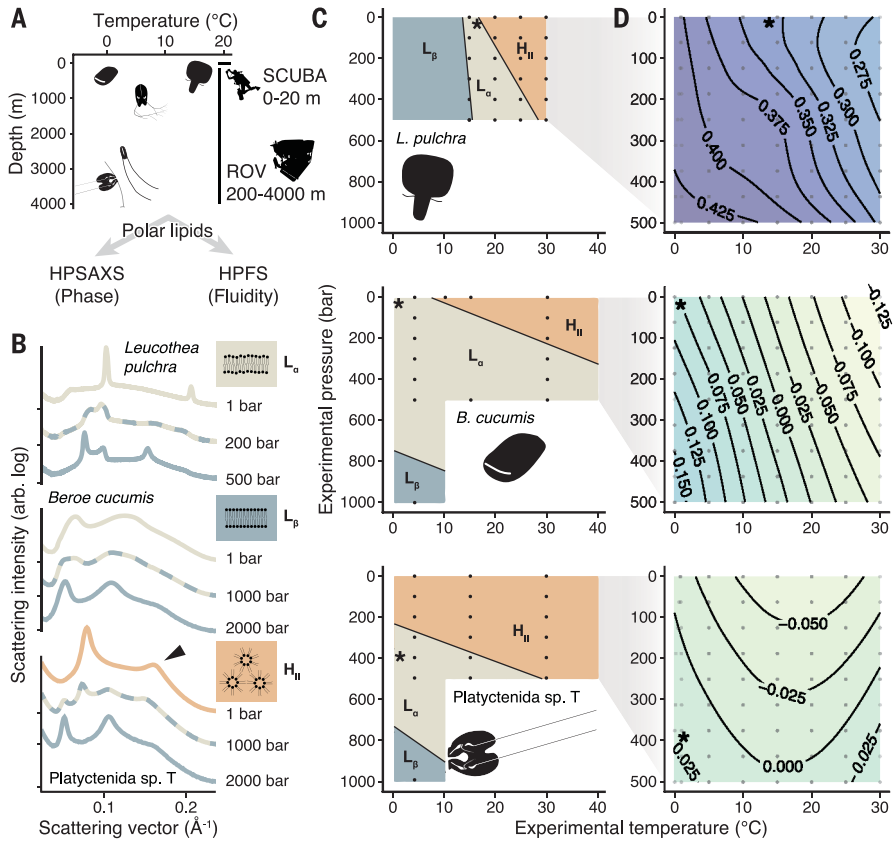

Fig. 2. Biophysical signatures of depth adaptation. (**A**) Schematic of the pipeline carried out on a set of ctenophores collected in different P-T regimes. Polar lipids were isolated from collected animals and analyzed by HPSAXS for phase properties and HPFS for membrane fluidity. (**B**) Representative SAXS profiles used to determine the phase of total polar lipid dispersions from the shallow Arctic ctenophore *B. cucumis* (profiles shown at 4°C), the deep-constrained Platyctenida sp. T (4°C), and the shallow-constrained *Leucothea pulchra* (15°C). Profiles are colored by phase composition, and baselines are offset for clarity. The broad peak indicated in Platyctenida sp. T results from the overlap of two close peaks characteristic of the H_{II} phase. The three main phases are shown in the inset cartoons. (**C**) Phase-change diagrams for the same dispersions based on SAXS data. Points mark measured states, and asterisks indicate the native P-T for each animal. (**D**) C-laurdan GP values for liposomes from the same samples measured across a P-T grid. Within lamellar phase regions, GP reflects lipid ordering, with lower values corresponding to more-fluid membranes. Near native conditions, GP pressure sensitivity was greater in shallow than in deep samples. This sensitivity is reflected by the proximity of contour lines.

depth-adaptive trend in lipid shape. The conical or cylindrical nature of a lipid's steric profile is captured in the monolayer spontaneous curvature parameter c_0. This curvature, which has units of inverse length, is defined as the reciprocal of the radius circumscribed by an unstressed monolayer of a given lipid. A negative-curvature lipid forms monolayers curving toward the headgroup, as are observed in the H_{II} phase, whereas a zero-curvature lipid forms flat monolayers, thus favoring lamellar phases. It has remained unclear whether the propensity for PPE to promote the H_{II} phase corresponds to a more negative c_0 (also called higher curvature) for the lipid class (*19*, *20*). We measured the pressure-dependent c_0 of PPE relative to that of diacyl PE using HPSAXS and found that it was more negatively curved under all conditions, requiring 700 bar of pressure to match the curvature of PE (Fig. 4B). PPE thus has the most negative curvature of any phospholipid class, although we cannot rule out other mechanisms by which it could promote the H_{II} phase. On the basis of these curvature values and previous measurements, we built a model that calculates the mean lipidome curvature at 1 bar, $\bar{c}_0$, incorporating contributions from headgroup classes (Fig. 4C), lysolipids, and *sn*-1 acyl chain structure (materials and methods). Modeled $\bar{c}_0$ becomes more negative with habitat depth among cold-adapted ctenophores (fig. S5C) as well as among all individuals (Fig. 4D). It does not correlate with temperature (Fig. 4D and fig. S5D). The model also predicts that in shallow-warm animals, PPE negative curvature is offset by positively curved lysolipids and lower chain unsaturation (fig. S5A).

The formula for $\bar{c}_0$ assumes ideal mixing of lipids, which is not the case in complex mixtures that typically compose cell membranes. To address this, we conducted molecular dynamics (MD) simulations of bilayers modeled after ctenophore lipidomes. Simulations were performed with all-atom resolution using the Chemistry at HARvard Macromolecular Mechanics v36 (CHARMM36) force field, which we were able to validate at high pressure (supplementary text) by predicting experimentally observed pressure-dependent changes to bilayer packing parameters and phase transitions (fig. S6). We constructed complex membranes containing representatives of the predominant (≥5%) lipid classes, including both phospholipids and cholesterol (fig. S7A). When comparing cold-adapted Platyctenida sp. T (4000 m, 2°C) with *Bolinopsis infundibulum* (10 m, 0°C)—whose lipidome is similar to that of *B. cucumis* used in HPSAXS (fig. S2E)—we observed similar pressure dependencies for lipid packing (APL strain) and translational mobility (D_T). However, the first moment of the lateral stress profiles—a measure of membrane deformability that is equal to the negative product of the monolayer bending modulus (k_b) and spontaneous curvature (c_0)—displayed a large (~500 bar) pressure offset (Fig. 4E). Although simulations were constrained to a bilayer state, the high $-k_b c_0$ values of Platyctenida sp. T lipids at low pressures were consistent with their tendency to form the nonlamellar H_{II} phase, as observed by HPSAXS.

We simulated two additional species from different P-T regimes: *Lampocteis cruentiventer* (630 m, 5°C) and *Bolinopsis vitrea* (10 m, 26°C) (fig. S7). The *L. cruentiventer* simulations produced APL strain and D_T values indistinguishable from those of the other two cold species and a smaller $-k_b c_0$ value compared with that of *B. infundibulum*. Because all simulations were done at 20°C and *L. cruentiventer* lives in a habitat warmer than those of *B. infundibulum* and Platyctenida sp. T, this difference could reflect the interplay between temperature and depth adaptation. In simulations, *B. vitrea* lipids exhibited the lowest values for $-k_b c_0$ across simulated pressures (fig. S7B), further indicating that lipidome components, including acyl chain composition, positively curved lipids, and cholesterol content, counterbalance the negative curvature of PPE in animals adapted to warm, shallow conditions. At 1000 bar, *B. vitrea* bilayers exhibited regions of condensed, gel-like chains (fig. S7D) that were not observed in the three cold-water species, consistent with the behavior of samples from the warmest shallow conditions analyzed by HPSAXS (Fig. 2C).

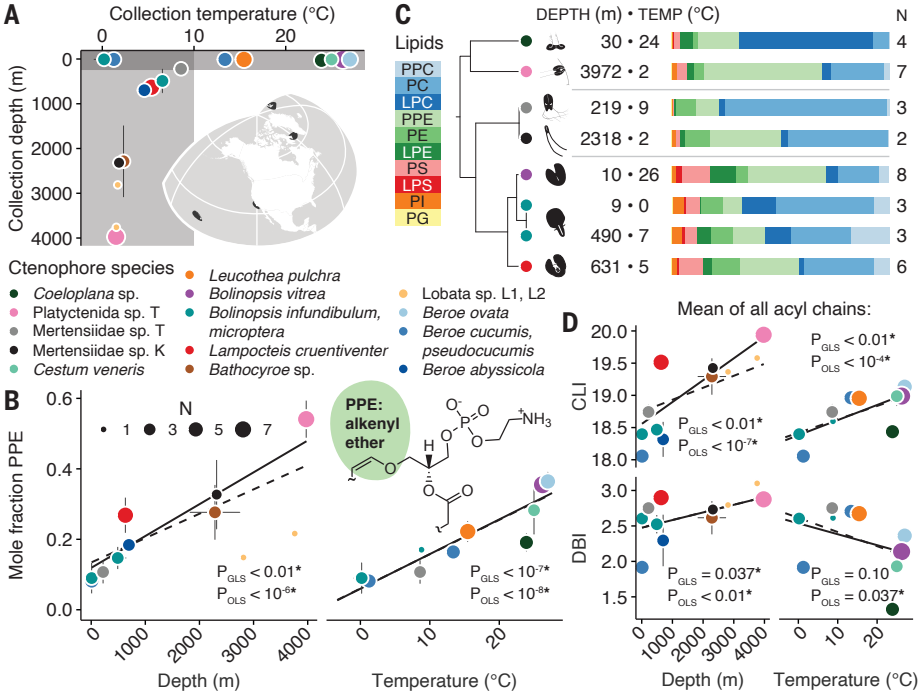

Fig. 3. Lipidomic analysis of ctenophore phospholipids. (**A**) Plot showing the depth and temperature regimes of the 66 ctenophores in the dataset. Each data point represents the mean for one of the 17 species collected; all error bars are ± SEMs. Subsets of the collections made ≤10°C and ≤250-m depth, shaded in gray, were used to assess depth and temperature trends, respectively. Collection locales are marked on the globe in black. (**B**) High relative abundance of PPE is correlated with both deep-cold and shallow-warm habitats. Structure of the PPE alkenyl ether linkage is inset. Ordinary least-squares regressions (OLS) (solid lines) and phylogenetically generalized ones (GLS) (dashed lines) are shown with their corresponding *P* values; an asterisk indicates significance at the $\alpha \leq 0.05$ level (Welch's *t* test). (**C**) Examples of independent lipidomic depth adaptation in three ctenophore clades, delimited with gray lines. Phylogenetics have revealed that ctenophores have depth specialized on multiple occasions. Within each clade, deeper cold species have higher fractions of PPE and PE and lower fractions of PC and lysolipids. Temperature specialization of a shallow, tropical representative of genus *Bolinopsis* is also shown. PPC, plasmenyl phosphatidylcholine; LPC, lysophosphatidylcholine; PS, phosphatidylserine; LPS, lysophosphatidylserine; PI, phosphatidylinositol. (**D**) Phospholipid total chain length index (CLI) and unsaturation [double bond index (DBI)] as a function of depth and temperature. Deeper cold lipidomes feature longer and more unsaturated acyl chains, whereas colder shallow lipidomes feature shorter and more unsaturated acyl chains. Regressions are shown as in (B).

On the basis of these analyses, we propose a homeocurvature adaptation model for depth specialization (Fig. 4F). In this model, phospholipids with more negative curvature (as measured at 1 bar) are required to maintain transmembrane protein function and membrane plasticity at higher pressure. In animals from deep, high-pressure environments, this requirement results in lipid compositions that do not form stable bilayers when depressurized. Consistent with this tradeoff, the increasing C-laurdan GP of disintegrating *Bathocyroe* [$\bar{c}_0 = -0.015 \pm 4.0 \times 10^{-3}$ Å^{-1} (SEM)] cell membranes in Fig. 1 resembled that of synthetic (fig. S3B) and animal-derived (Fig. 2D and fig. S1F) liposomes inverting to form H_{II}. By contrast, the shallow-constrained species *Bolinopsis microptera* [$\bar{c}_0 = -0.0052 \pm 1.2 \times 10^{-3}$ Å^{-1} (SEM)], which does not disintegrate, showed a decrease in GP under the same conditions, consistent with its membranes remaining lamellar and becoming more fluid as they were warmed (Fig. 1C and fig. S8A).

Modulating lipid curvature can enhance or reduce biological pressure tolerance

We sought to test the key prediction of the homeocurvature adaptation model—that lipidome curvature modulates biological pressure tolerance—using laboratory organisms with membrane compositions that could be genetically manipulated. The inner membrane of *E. coli* strain K12 is composed primarily of PE, with acyl chains that maintain both fluidity (*4*) and curvature (*5*) in response to temperature changes. To test the effects of more-negative lipidome curvature, we expressed a PPE synthesis cassette (plsAR) from *Clostridium perfringens* (*21*) in anaerobically grown *E. coli* strain BL21 (Fig. 5A) and then exposed the cultures to high pressure for 48 hours. Upon induction of plsAR expression, 25% of total phospholipids were converted from PE to PPE (fig. S9A), whereas the acyl chain profile remained similar (fig. S9B). SAXS analysis of reconstituted *E. coli* lipid extracts showed that plsAR expression promoted the H_{II} phase relative to the empty-vector control, consistent with an increase in negative phospholipid curvature (Fig. 5B and fig. S9C). When incubated at 500 bar, both the doubling rate and survival of PPE-synthesizing cells were significantly less pressure sensitive compared with those of the empty-vector control (Fig. 5, C and D).

To test the effects of reduced negative lipidome curvature on high-pressure fitness, we used a P_{BAD}-PC synthase cassette (*22*) to replace PE with PC. PC has a higher fluidity than PE and better resists pressure-induced gelling (fig. S3D), but its cylindrical profile inhibits nonlamellar topologies (*23*, *24*). It can thus be used to differentiate the effects of membrane fluidity and gel phase transitions from those related to curvature. SAXS analysis confirmed that lipids from PC-synthesizing cells were unable to form the H_{II} phase but were more resistant to the gel phase transition (Fig. 5F and fig. S9C). Growth of PC-producing cells was diminished at 250 bar, and survival ceased at 500 bar (Fig. 5, G and H), which indicates that the loss of lipid curvature is deleterious to high-pressure fitness even when fluidity is increased. Both PC- and PPE-synthesizing strains also showed lower levels of phosphatidylglycerol (PG), but loss of PG synthesis alone did not alter high-pressure fitness under our experimental conditions (fig. S9, D and E). Therefore, increase (by PPE synthesis) or decrease (by PC synthesis) of negative lipidome curvature can be sufficient to modulate high-pressure fitness in cells.

Discussion

All biological membranes consist of cylindrical bilayer-forming lipids, which support membrane structure, and conical nonbilayer lipids, which support membrane plasticity (*25*). The high-pressure and low-temperature waters of the deep sea present a biophysical challenge to maintaining the latter. Reconstituted deep-sea lipids can adopt nonlamellar topologies, such as the H_{II} phase, even under these extreme conditions. Multiple molecular adaptations underlie this capability. The ether phospholipid PPE, a major component of deep-sea ctenophore membranes, maintains a conical shape under high-pressure conditions because of its highly negative spontaneous curvature. We also observed increased abundance of PPE in tropical surface animals, where it could fulfill roles as an antioxidant (*26*) and as a driver of local heterogeneity in cholesterol-rich membranes (*27*). Exclusive to samples from deep waters was the combination

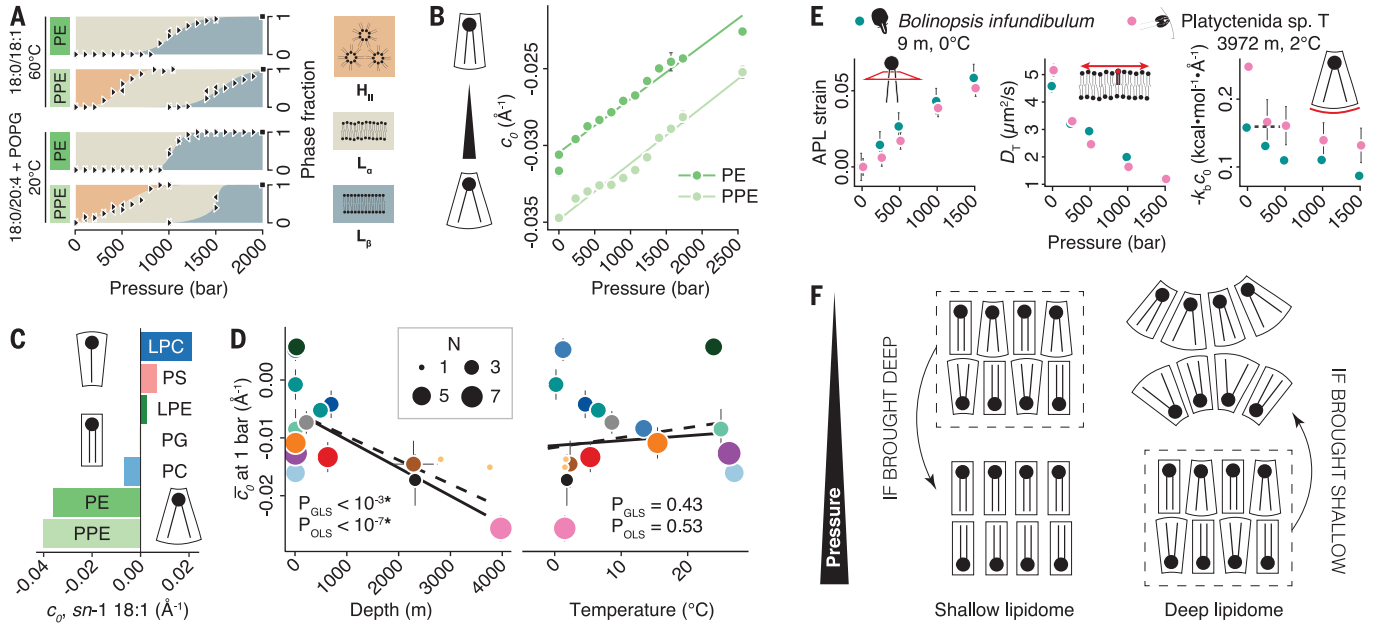

Fig. 4. Exploring the role of lipid curvature in deep-sea lipidomes enriched in PPE. (**A**) Lipid phase ratios estimated from HPSAXS data plotted as a function of pressure and of the PPE headgroup. At the temperatures tested, PPE was H_{II} phase and PE was L_α phase at 1 bar regardless of whether the *sn*-2 acyl chain was poly- or monounsaturated. The polyunsaturated phospholipids were chosen as the closest commercially available analogs to those in ctenophores; 5 mol % PG was added to bring the inverted phase transition within an instrumentally achievable P-T domain. Each black triangle denotes an individual x-ray exposure taken during a pressure sweep in the indicated direction. Black squares at the upper right are exposures taken at maximum pressure. (**B**) Spontaneous curvature (c_0) values measured for PPE and PE species with a monounsaturated *sn*-2 chain. Cartoons by the vertical axis illustrate the relationship between c_0 and lipid shape. PPE shows a stronger negative curvature than PE, and the effect of pressure on both is identical. Neutral-plane c_0 was derived from HPSAXS profiles of the lipids (20%) hosted in a di-oleoyl PE (DOPE) H_{II} phase and relaxed with 10.7% w/w 9(Z)-tricosene. (**C**) Representative c_0 values for phospholipid classes. These were used along with linear corrections for *sn*-1 acyl chain structure (materials and methods) to estimate the mean phospholipid curvature at 1 bar ($\bar{c}_0$) for all measured lipidomes. (**D**) The robust correlation of $\bar{c}_0$ with habitat depth among all animals sampled; deeper lipidomes feature a higher degree of lipidome curvature. Habitat temperature does not predict $\bar{c}_0$. Regressions are shown as in Fig. 3. (**E**) Comparison of simulated lipidomes modeled after a cold, shallow species (*B. infundibulum*) and a deep species (Platyctenida sp. T). Pressure-dependent properties include area per lipid (APL) strain relative to 1 bar, average lipid translational diffusion rate (D_T), and the first moment of the computed lateral stress profile, which is equal to $-k_b c_0$. All simulations were run at 20°C. For $-k_b c_0$, the pressure equivalency of shallow and deep systems is indicated with a dashed line. Simulation snapshots and additional details are shown in fig. S7. (**F**) A homeocurvature adaptation model in which a more negative baseline (1 bar) lipidome curvature is required to offset the effects of high pressure on lipid shape. For lipidomes of both shallow- and deep-living species, physiological membrane states (dashed boxes) contain a mixture of bilayer and nonbilayer lipids, but the chemistry of these species must differ to maintain this arrangement. When membranes from shallow-living animals were compressed, lipidome curvature was lost, potentially disrupting membrane dynamics and plasticity. When membranes from deep-living animals were decompressed, negative lipidome curvature increased, destabilizing membrane structure.

of abundant PPE, long and highly unsaturated acyl chains, and low amounts of lysolipids, all of which contribute to lipidomes with exceptionally negative spontaneous curvature at 1 bar. High pressure reduces this extreme curvature so that deep lipidomes form physiologically viable membranes under their native conditions.

Lipid adaptation in marine systems has mostly been explored in the context of temperature, with pressure and cold adaptation treated as functionally interchangeable. However, pressure is a stronger inhibitor of nonlamellar topologies because of their large molar volumes. By contrast, temperature is dominant in controlling membrane fluidity and the formation of gel phases. Accordingly, we found that depth adaptation in ctenophores is biochemically distinct from cold adaptation. The hallmark of shallow, low-temperature lipidomes is a high fraction of low–melting temperature PC lipids with shorter acyl chains, whose abundance decreases with depth. By contrast, deep-sea animals accumulate conical nonbilayer lipids, including PPE, which has both stronger curvature and greater fluidity compared with diacyl PE. These differing responses to cold and pressure suggest that deeper environments might not substitute for contracting regions with cold surface waters, which has been proposed as a mechanism of ecological resilience in warming polar seas (*28*).

The homeocurvature adaptation model postulates that pressure-induced changes in lipid shape are relevant to the habitat ranges of both shallow and deep animals (Fig. 4F). The loss of motor function in shallow-constrained animals subjected to high pressure (movie S1 and fig. S1, A and B) is consistent with membrane-associated defects in the nervous system, for example in synaptic vesicle trafficking or ion channel function. Animals specialized to deep habitats may mitigate such defects by accumulating high-curvature lipids, which are also enriched in the nervous systems of mesophiles (*29*). Because it is based on hydrocarbon compressibility, the effect of pressure on lipid shape is similar in all phospholipids, so counteracting it requires a more negative baseline (1 bar) curvature that may not sustain a lamellar phase at the surface. Through this mechanism, adaptation to extreme depths could have given rise to organisms that require pressure to maintain their membranes.

REFERENCES AND NOTES

1. P. H. Yancey, M. E. Gerringer, J. C. Drazen, A. A. Rowden, A. Jamieson, *Proc. Natl. Acad. Sci. U.S.A.* **111**, 4461–4465 (2014).
2. G. N. Somero, *Annu. Rev. Physiol.* **54**, 557–577 (1992).
3. A. R. Cossins, A. G. Macdonald, *J. Bioenerg. Biomembr.* **21**, 115–135 (1989).

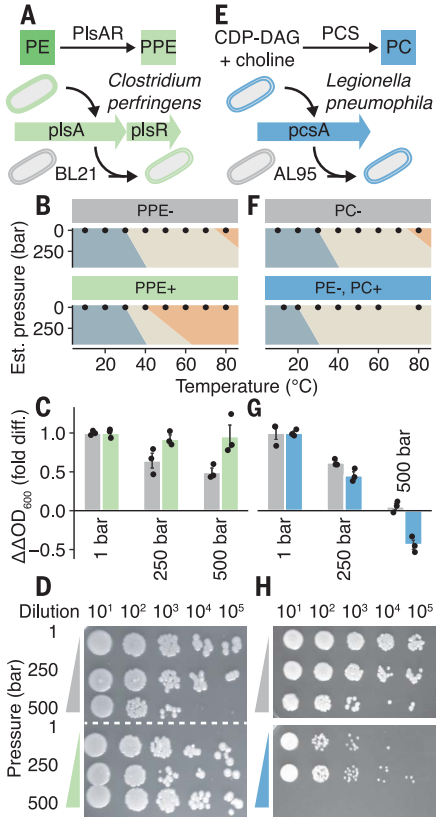

Fig. 5. Testing the principles of pressure adaptation in engineered bacterial cells. (**A**) Heterologous synthesis of PPE, using plasmid-based expression of the plsAR PE reductase from *Clostridium*, enhances *E. coli* lipidome curvature and its propensity to invert into H_{II}, as assayed by SAXS as a function of temperature. (**B**) Phase diagrams of *E. coli* polar lipids (inner and outer membrane) in PPE− (BL21 + pET28a; gray) and PPE+ (BL21 + pPlScp; green) strains. To facilitate comparison with the pressure treatments, these diagrams are extrapolated along a pressure axis using published temperature-pressure equivalencies (*24*). (**C**) Growth of PPE-lacking and PPE-containing *E. coli* in microaerobic culture under pressure. The difference in pressure sensitivity of growth was significant (P = 0.009, multiple regression with F test). (**D**) Postdecompression survival was similarly rendered pressure insensitive by PPE (compare lower right colonies in both panels). (**E**) Non-native synthesis of PC, using plasmid-based expression of the PC synthase (PCS) from *Legionella* in the PE-free background AL95, reduces lipidome curvature and propensity to invert into H_{II}. (**F**) Pressure-extrapolated phase diagrams of *E. coli* polar lipids in PC− (AAL9256 with an integrated P_{BAD}-pssA cassette; gray) and PE−, PC+ (AL95 + pPCSlp; blue) strains. (**G** and **H**) Growth (G) and survival (H) were assessed as in (C) and (D), except that outgrowth before pressurization was aerobic. The difference in pressure sensitivity of growth was significant (P = 0.002), and the PC strain was inviable at 500 bar. Strain pairs were chosen to minimize differences in genetic background, and promoters were identical within each pair.

4. M. Sinensky, *Proc. Natl. Acad. Sci. U.S.A.* **71**, 522–525 (1974).
5. S. Morein, A. Andersson, L. Rilfors, G. Lindblom, *J. Biol. Chem.* **271**, 6801–6809 (1996).
6. M. Wikström *et al.*, *J. Biol. Chem.* **284**, 954–965 (2009).
7. P. I. Kuzmin, J. Zimmerberg, Y. A. Chizmadzhev, F. S. Cohen, *Proc. Natl. Acad. Sci. U.S.A.* **98**, 7235–7240 (2001).
8. J. R. Winnikoff, S. H. D. Haddock, I. Budin, *J. Exp. Biol.* **224**, jeb242800 (2021).
9. G. L. Kooyman, *Diverse Divers: Physiology and Behavior*, vol. 23 of *Zoophysiology* (Springer, 1989).
10. P. Burkhardt *et al.*, *Science* **380**, 293–297 (2023).
11. S. Takamori *et al.*, *Cell* **127**, 831–846 (2006).
12. M. E. Gerringer *et al.*, *R. Soc. Open Sci.* **4**, 171063 (2017).
13. J. J. Childress, A. T. Barnes, L. B. Quetin, B. H. Robison, *Deep Sea Res.* **25**, 419–422 (1978).
14. D. K. Rai *et al.*, *J. Appl. Cryst.* **54**, 111–122 (2021).
15. J. M. Dean, I. J. Lodhi, *Protein Cell* **9**, 196–206 (2018).
16. R. Dawaliby *et al.*, *J. Biol. Chem.* **291**, 3658–3667 (2016).
17. J. H. Lorent *et al.*, *Nat. Chem. Biol.* **16**, 644–652 (2020).
18. P. E. Glaser, R. W. Gross, *Biochemistry* **33**, 5805–5812 (1994).
19. K. Lohner, P. Balgavy, A. Hermetter, F. Paltauf, P. Laggner, *Biochim. Biophys. Acta* **1061**, 132–140 (1991).
20. K. Lohner, *Chem. Phys. Lipids* **81**, 167–184 (1996).
21. D. R. Jackson *et al.*, *ACS Chem. Biol.* **16**, 6–13 (2021).
22. M. Bogdanov, P. Heacock, Z. Guan, W. Dowhan, *Proc. Natl. Acad. Sci. U.S.A.* **107**, 15057–15062 (2010).
23. R. Winter *et al.*, in *High Pressure Effects in Molecular Biophysics and Enzymology*, J. L. Markley, D. B. Northrop, C. A. Royer, Eds. (Oxford Univ. Press, 1996), pp. 274–297.
24. P. T. C. So, S. M. Gruner, S. Erramilli, *Phys. Rev. Lett.* **70**, 3455–3458 (1993).
25. S. M. Gruner, *Proc. Natl. Acad. Sci. U.S.A.* **82**, 3665–3669 (1985).
26. A. Broniec *et al.*, *Free Radic. Biol. Med.* **50**, 892–898 (2011).
27. L. J. Pike, X. Han, K.-N. Chung, R. W. Gross, *Biochemistry* **41**, 2075–2088 (2002).
28. D. Cottin *et al.*, *Comp. Biochem. Physiol. A Mol. Integr. Physiol.* **162**, 357–363 (2012).
29. X. Han, D. M. Holtzman, D. W. McKeel Jr., *J. Neurochem.* **77**, 1168–1180 (2001).
30. J. Winnikoff, octopode/homeocurvature-2024: 20240422a, Zenodo (2024); https://doi.org/10.5281/zenodo.11029505.

ACKNOWLEDGMENTS

S. Gruner, G. Somero, D. Bartlett, and P. Girguis contributed discussions that informed the direction of this work. C. Webster, C. Havermans, S. Meyer, L. Christianson, S. Johnson, and D. Schultz collected ctenophores for this study. Crews of the *R/V Western Flyer*, *R/V Rachel Carson*, *R/V Ka'imikai-O-Kanaloa*, *R/V Kilo Moana*, ROV Doc Ricketts, ROV Ventana, and MBARI's MiniROV provided field support. Q. Huang and G. Pabst provided SAXS technical and analytical support. W. Dowhan, M. Bogdanov, and J. Clardy provided bacterial strains and plasmids. **Funding:** The work was supported by the National Science Foundation (MCB-2046303, MCB-2316458, and IOS-2040022 to I.B.; DEB-1542679, OCE-1829805, and MCB-2316456 to S.H.D.H.; and MCB-2121854 and MCB-2316457 to E.L.); NASA (postdoctoral fellowship 0017-NPP-MAR22-A-Astrobio to J.R.W.); the Office of Naval Research (N00014-23-1-2543 to I.B.); the National Institutes of Health (GM139641 to E.A.D.; 5T32EB009380-14 to D.M.; and 1ZIAHD008955 to A.S.); and the David and Lucile Packard Foundation. SAXS data acquisition was performed at the Cornell High Energy Synchrotron Source, which is supported by the National Science Foundation (DMR-1829070); the National Institutes of Health (1-P30-GM124166-01A1); and the New York State Foundation for Science, Technology and Innovation. **Author contributions:** Conceptualization: J.R.W., S.H.D.H., and I.B. Methodology: J.R.W., A.M.A., O.Q., A.S., R.E.G., E.L., and I.B. Investigation: J.R.W., D.M., S.J.V.-U., M.A.P.-J., A.M.A., O.Q., A.S., R.E.G., E.L., S.H.D.H., and I.B. Visualization: J.R.W., D.M., E.L., S.H.D.H., and I.B. Funding acquisition: E.A.D., E.L., S.H.D.H., and I.B. Project administration: J.R.W., S.H.D.H., and I.B. Supervision: E.A.D., E.L., S.H.D.H., and I.B. Writing – original draft: J.R.W. and I.B. Writing – review & editing: J.R.W., D.M., E.L., S.H.D.H., and I.B. **Competing interests:** The authors declare that they have no competing interests. **Data and materials availability:** Raw data, analysis, and visualization code are archived at Zenodo (*30*). **License information:** Copyright © 2024 the authors, some rights reserved; exclusive licensee American Association for the Advancement of Science. No claim to original US government works. https://www.science.org/about/science-licenses-journal-article-reuse

SUPPLEMENTARY MATERIALS

science.org/doi/10.1126/science.adm7607
Materials and Methods
Supplementary Text
Figs. S1 to S10
Tables S1 to S3
References (*31*–*81*)
MDAR Reproducibility Checklist
Movie S1
Data S1

Submitted 6 November 2023; accepted 17 May 2024
10.1126/science.adm7607